Mech. Sci., 8, 369–383, 2017
https://doi.org/10.5194/ms-8-369-2017
© Author(s) 2017. This work is distributed under
the Creative Commons Attribution 3.0 License.

Mechanical Sciences
Open Access

The design formulae for skew line gear wheel structures oriented to the additive manufacturing technology based on strength analysis

Yueling Lyu, Yangzhi Chen, and Yifan Lin

School of Mechanical and Automotive Engineering, South China University of Technology, Guangzhou 510640, China

Correspondence: Yangzhi Chen (meyzchen@scut.edu.cn)

Received: 30 March 2017 – Revised: 26 August 2017 – Accepted: 10 November 2017 – Published: 14 December 2017

Abstract. In this paper, the design methodology for a skew line gear pair oriented to additive manufacturing technology, with an one-tooth driving line gear and its coupled driven line gear, used for the conventional powered transmission, is researched based on strength analysis. First, the expressions of meshing forces on the line tooth of line gears are deduced; the deformations and stresses of existing structures of a line gear pair are analyzed by using ANSYS Workbench. Then, the reliable structure and the parameters standardization formulae of a line gear pair are deduced by stiffness and strength analyses. Finally, a design case shows that the proposed design methods provide a convenient and reasonable design tool for designing a skew line gear pair in conventional powered transmission field.

1 Introduction

A Line Gear (LG), based on the space curve meshing theory, is an innovative gear proposed by Yangzhi Chen (Chen, 2014). With a large transmission ratio, light weight and small size, a LG pair is mainly applicable to small and micro mechanical systems, such as: toy industry, instruments and apparatus and new energy installation. The LG was also named as Space Curve Meshing Wheel (SCMW) or Micro Elastic Meshing Wheel (MEMW) in previous studies, including the Micro-elastic Meshing Wheel (MEMW) (Chen et al., 2009), Arbitrary Intersecting Gear (AIG) (Chen et al., 2013a) and Space Curve Meshing Skew Gear (SCMSG) (Chen et al., 2013b). The previous researches mainly focused on MEMW and AIG covering their meshing theory, manufacture technology, geometric design formula, sliding rate, strength analysis and transmission error analysis (Chen, 2014).

Strength analysis is an integral part of any mechanical design, especially for gear (Patil et al., 2014; Huang et al., 2013; Pedrero et al., 2007; Chang et al., 2000; Wei et al., 2011). Similarly, strength analysis for line gear wheel is also essential, especially for the line gear pair applied in the traditional machine, because the existing structure of the line gear pair is easy to be deformed in application of large transmission torque of traditional machine (Chen, 2014; Chen et al., 2009, 2013a, b). When the number of the line tooth of a driving line gear is 1, a line gear pair can obtain bigger transmission ratio. However, the length of the line tooth increases because the contact ratio must be more than 1 (Chen and Chen, 2012; Lv et al., 2015), which means the strength and stiffness of the line gear are not enough to work, and a new structure of the line gear wheel needs to be designed on demand. Additive Manufacturing technology (Frederik et al., 2013) has been developing rapidly in the past decades. It is widely used because it can produce a variety of shapes of products, and its manufacturing cost is proportional to the real weight of the product. Additive manufacturing technology is used as a main manufacturing technology for the LG so far (Yang et al., 2009).

In this paper, oriented to the additive manufacturing technology, a skew line gear pair, whose number of the line tooth of the driving line gear is 1, is designed to improve its strength and overall stiffness, to reduce its volume and manufacturing cost, which is applicable to traditional powered mechanical transmission field. First, the expressions of meshing forces on the line tooth of the skew line gears at

different meshing points are deduced. Then the deformations and stresses of the existing structure of the line gears, when the number of the line tooth of a driving line gear is 1, are analyzed by using ANSYS Workbench. Moreover, the driven line gear wheel structure is optimized using less material as design objective, namely, the design formula of the thickness of a hollow truncated cone on the basis of the stiffness criterion is deduced, and the calculation formula of the thickness of the optimal ribbed slab is derived on the basis of the strength criterion, and the experience formulae of the thicknesses of a top circle plate and a bottom circle plate are deduced. Then, the calculation formulae of the driving line gear wheel are deduced according to the strength and stiffness criterion. Finally, an example is designed to confirm the rationality of the standardization formulae. This paper provides a basic theory for the skew line gear pair applied in conventional powered transmission field.

2 The meshing forces of a line gear pair

According to previous work of co-author (Chen and Chen, 2012), the equation of contact ratio ε is $\Delta t N_1/(2\pi)$, where N_1 is the number of a driving line tooth; Δt is the design parameter of line gear. Therefore, if the number of a driving line tooth N_1 equals to 1 and the contact ratio of a line gear pair is more than 1, the design parameter Δt should be equal to 2π, and the length of line teeth is much longer. Suppose $c = 12$ mm, $\theta = 155°$, $m = 5$ mm, $n = 6$ mm, $a = 36.2373$ mm, $b = -58.8615$ mm, $t_s = -3.5\pi$, $N_1 = 1$ and $\Delta t = 2\pi$, then a line gear pair is designed, as shown in Fig. 1. In the following discussion, the subscript 1 refers to the driving line gear while 3 refers to the driven line gear.

2.1 The meshing forces on a driving line tooth

Suppose a given power is P, and a rotating speed is ω_1, then the torque can be obtained:

$$T_1 = \frac{P}{\omega_1} \tag{1}$$

For a driving line tooth, the radius of torque is R_{T_1}, and $R_{T_1} = m$, so the meshing force on the driving line tooth at the meshing point is:

$$F_1 = \frac{T_1}{R_{T_1}} \tag{2}$$

The value of the meshing force on the direction of the binormal vector on a driving line tooth is as Eq. (3) and its direction is contrary to the direction of the binormal vector, where λ_1 is the helix height of the driving contact curve, $\lambda_1 = \arctan(n/m)$.

$$F_n = F_1 \sin\lambda_1 \tag{3}$$

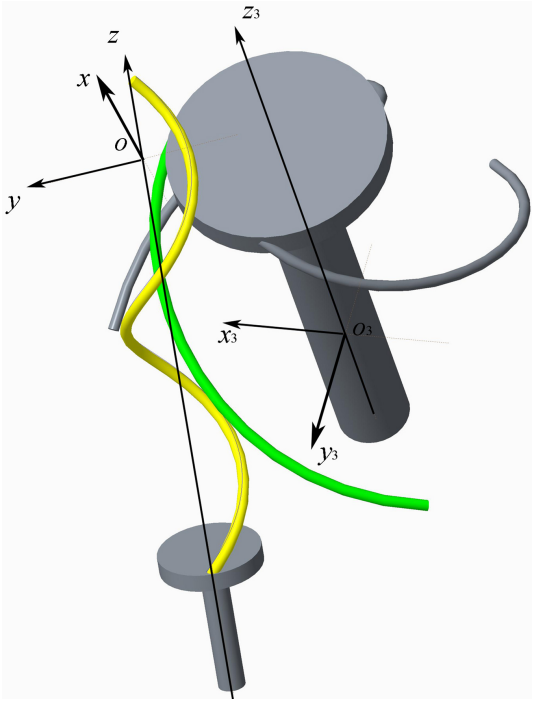

Figure 1. A skew line gear pair when the number of driving line tooth is 1.

The direction of the binormal vector of a driving tooth is as Eq. (4), where t is parameter in the range of that $t_s \le t \le t_e$.

$$\boldsymbol{r}^{(1)} = \begin{bmatrix} \frac{n\sin t}{\sqrt{n^2+m^2}} \\ \frac{-n\cos t}{\sqrt{n^2+m^2}} \\ \frac{m}{\sqrt{n^2+m^2}} \end{bmatrix} \tag{4}$$

The meshing force on a driving line tooth at the meshing point is as Eq. (5).

$$F_n^{(0)} = F_n r^{(1)} \tag{5}$$

Substituting Eq. (4) into Eq. (5), Eq. (6) can be obtained.

$$\boldsymbol{F}_n^{(0)} = F_n \begin{bmatrix} \frac{-n\sin t}{\sqrt{n^2+m^2}} \\ \frac{n\cos t}{\sqrt{n^2+m^2}} \\ \frac{-m}{\sqrt{n^2+m^2}} \end{bmatrix} \tag{6}$$

2.2 The meshing force on a driven line tooth

The meshing force's value on a driven line tooth is F_n, and the force's direction is the same as the direction of the binormal vector on a driving tooth, so the meshing force's expression $F_3^{(1)}$ on a driven line tooth in $o_1 - x_1y_1z_1$ is obtained as

Eq. (7).

$$\boldsymbol{F}_3^{(1)} = F_n \begin{bmatrix} \dfrac{n\sin t}{\sqrt{n^2+m^2}} \\ \dfrac{-n\cos t}{\sqrt{n^2+m^2}} \\ \dfrac{m}{\sqrt{n^2+m^2}} \end{bmatrix} \tag{7}$$

The meshing force's expression $F_3^{(q)}$ on a driven line tooth in $o_3 - x_3y_3z_3$ is obtained as Eq. (8).

$$\boldsymbol{F}_3^{(q)} = \mathbf{M}_{31} F_n \begin{bmatrix} \dfrac{n\sin t}{\sqrt{n^2+m^2}} \\ \dfrac{-n\cos t}{\sqrt{n^2+m^2}} \\ \dfrac{m}{\sqrt{n^2+m^2}} \end{bmatrix} \tag{8}$$

Where $\mathbf{M}_{31} = \mathbf{M}_{3q}\mathbf{M}_{q1}$; ϕ_1 and ϕ_3 are the rotational angle of the driving and driven line gear, respectively; in Chen et al. (2013b), when $0° < \theta < 90°$, then,

$$\mathbf{M}_{31} = \begin{bmatrix} -\cos\theta\cos\phi_3\cos\phi_1 + \sin\phi_3\sin\phi_1 & -\cos\theta\cos\phi_3\sin\phi_1 - \sin\phi_3\cos\phi_1 & -\sin\theta\cos\phi_3 & (-a\cos\theta + b\sin\theta)\cos\phi_3 - c\sin\phi_3 \\ -\cos\theta\sin\phi_3\cos\phi_1 - \cos\phi_3\sin\phi_1 & -\cos\theta\sin\phi_3\sin\phi_1 + \cos\phi_3\cos\phi_1 & -\sin\theta\sin\phi_3 & (-a\cos\theta + b\sin\theta)\sin\phi_3 - c\cos\phi_3 \\ \sin\theta\cos\phi_1 & \sin\theta\sin\phi_1 & -\cos\theta & a\sin\theta + b\cos\theta \\ 0 & 0 & 0 & 1 \end{bmatrix} \tag{9}$$

when $90° < \theta < 180°$, then

$$\mathbf{M}_{31} = \begin{bmatrix} -\cos\theta\cos\phi_3\cos\phi_1 - \sin\phi_3\sin\phi_1 & -\cos\theta\cos\phi_3\sin\phi_1 + \sin\phi_3\cos\phi_1 & -\sin\theta\cos\phi_3 & (-a\cos\theta + b\sin\theta)\cos\phi_3 - c\sin\phi_3 \\ \cos\theta\sin\phi_3\cos\phi_1 - \cos\phi_3\sin\phi_1 & \cos\theta\sin\phi_3\sin\phi_1 + \cos\phi_3\cos\phi_1 & \sin\theta\sin\phi_3 & (-a\cos\theta + b\sin\theta)(-\sin\phi_3) - c\cos\phi_3 \\ \sin\theta\cos\phi_1 & \sin\theta\sin\phi_1 & -\cos\theta & a\sin\theta + b\cos\theta \\ 0 & 0 & 0 & 1 \end{bmatrix} \tag{10}$$

According to the space curve meshing theory (Chen et al., 2013b), a space curve meshing equation can be obtained as Eq. (11) from a given driving contact curve equation.

$$\begin{aligned} &c\cos\theta\cos(\phi_1 - t) - a\cos\theta\sin(\phi_1 - t) \\ &\quad -(n\pi + nt - b)\sin(\phi_1 - t) = 0 \end{aligned} \tag{11}$$

Substituting Eqs. (9) and (10) into Eq. (8), Eqs. (12) and (13) can be obtained. When $0° < \theta < 90°$,

$$\boldsymbol{F}_3^{(q)} = F_n \begin{bmatrix} \dfrac{\sin(\phi_1 - t)n\cos\theta\cos\phi_3}{\sqrt{n^2+m^2}} + \dfrac{\cos(\phi_1 - t)n\sin\phi_3}{\sqrt{n^2+m^2}} - \dfrac{m\sin\theta\cos\phi_3}{\sqrt{n^2+m^2}} \\ \dfrac{\sin(\phi_1 - t)n\cos\theta\sin\phi_3}{\sqrt{n^2+m^2}} - \dfrac{\cos(\phi_1 - t)n\cos\phi_3}{\sqrt{n^2+m^2}} - \dfrac{m\sin\theta\sin\phi_3}{\sqrt{n^2+m^2}} \\ -\dfrac{\sin(\phi_1 - t)n\sin\theta}{\sqrt{n^2+m^2}} - \dfrac{m\cos\theta}{\sqrt{n^2+m^2}} \end{bmatrix} \tag{12}$$

when $90° < \theta < 180°$,

$$\boldsymbol{F}_3^{(q)} = F_n \begin{bmatrix} \dfrac{\sin(\phi_1 - t)n\cos\theta\cos\phi_3}{\sqrt{n^2+m^2}} - \dfrac{\cos(\phi_1 - t)n\sin\phi_3}{\sqrt{n^2+m^2}} - \dfrac{m\sin\theta\cos\phi_3}{\sqrt{n^2+m^2}} \\ -\dfrac{\sin(\phi_1 - t)n\cos\theta\sin\phi_3}{\sqrt{n^2+m^2}} - \dfrac{\cos(\phi_1 - t)n\cos\phi_3}{\sqrt{n^2+m^2}} + \dfrac{m\sin\theta\sin\phi_3}{\sqrt{n^2+m^2}} \\ -\dfrac{\sin(\phi_1 - t)n\sin\theta}{\sqrt{n^2+m^2}} - \dfrac{m\cos\theta}{\sqrt{n^2+m^2}} \end{bmatrix} \tag{13}$$

2.3 Deformation of the existing structure for a line gear pair

In Fig. 1, suppose the torque of a driving line gear is 2 N m, and $R_{T_1} = 5$ mm, then the meshing force's value on the driving line gear is $F_1 = 400$ N, and the meshing force's value on the direction of the binormal vector on the driving line tooth at the ending meshing point is 2.779429 N, which in $o_1 - x_1y_1z_1$ is [−213.5216 N 3.9223×10^{-14} N −177.9347 N]. The meshing force on the direction of the binormal vector on the driven line tooth at the initial meshing point in $o_3 - x_3y_3z_3$ is [−116.1131 N −161.5928 N 194.0561 N]. The material of the following line gear is structural steel and its mechanic properties are $E = 2.0 \times 10^{11}$ Pa, $\mu = 0.3$, $\sigma_s = 2.6 \times 10^8$ Pa. The statics analysis results on the driving and the driven line gears are shown in Fig. 2 by using ANSYS Workbench. Their boundary conditions are the fixed upper surface of the line gear wheels. The load distribution are applied on the end of the tines.

In Fig. 2, the maximum deflection of the driving line gear is 0.316 m, and the maximum equivalent stress is 5.884×10^{10} Pa, while the maximum deflection of the driven line gear is 0.22902 m, and the maximum equivalent stress is 2.8469×10^{10} Pa. It can be concluded that the deflections of line gears are so large and beyond elastic deformation allowance that the line gear pair cannot meet the transmission requirement. Therefore, a new structure for a line gear pair must be proposed to improve the stiffness of line gear and to ensure the transmission accuracy in traditional powered transmission field. The design methods and formulae of the line gear wheels in this paper are researched oriented to additive manufacturing technology.

3 Novel structures for the line gear wheel oriented to additive manufacturing technology

The number of the driving line tooth is 1 in this paper. According to Sect. 2.3, it can be concluded that the stiffness of the structure of a line gear pair is so low that the line gear pair cannot meet the transmission requirement, which was designed as a structure in Fig. 1.

New structure of a line gear pair is proposed in entity type as shown in Fig. 3, the stiffness and strength of the line gear pair should be improved much more.

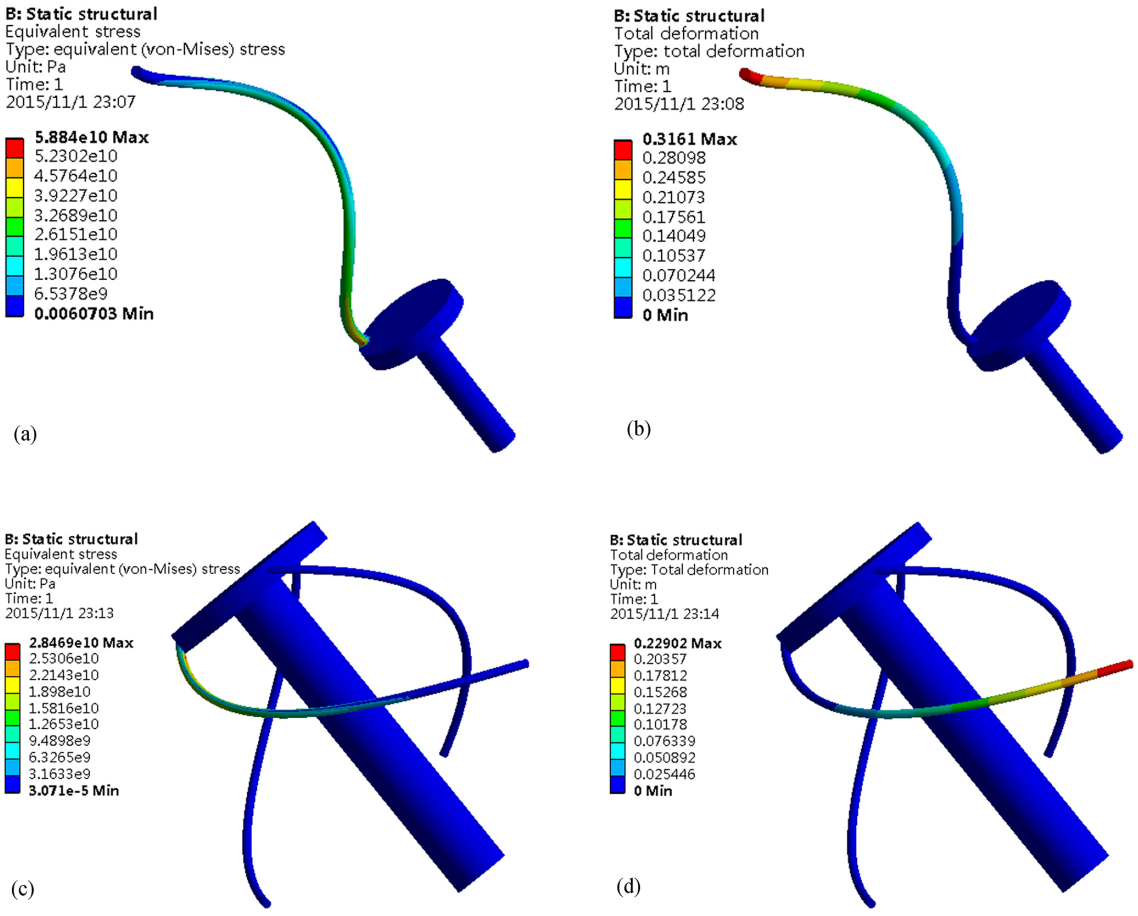

Figure 2. Statics analysis of a skew line gear pair with existing structure.

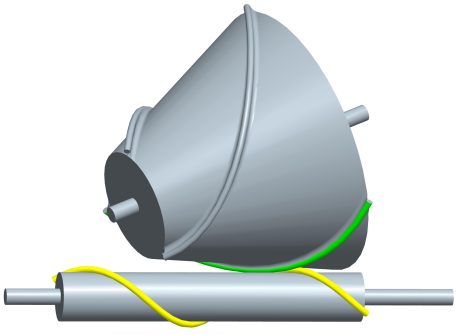

Figure 3. The structures of line gear pair are proposed in entity type.

However, oriented to the additive manufacturing technology, the greater the weight of the wheel is, the greater its production cost is. Therefore, under meeting the requirement of stiffness and strength, it can be considered to remove part of material from the entity structure of the line gear wheel in order to reduce the manufacturing cost of the line gear. Without doubt, it can directly use the entity type as structure of the line gear wheel when the size of the line gear pair is small while it also needs to transmit larger power. In this paper, the size of line gear is designed in the range of $\sim$ 5–200 mm. The radius of the driving line gear wheel is relatively small and the structure of the driving line gear wheel can be designed as an entity type. The radius of a driven line gear wheel depends on the fundamental dimensions, such as the offset of two skewed axes c, the transmission ratio i, the angle of two skewed axes θ. When the overall size of a driven line gear is relative larger, a hollow truncated cone structure is proposed to be the mainly driven line gear wheel structure, as shown in Fig. 4. Because the meshing force of the driven line tooth acts on the ektexine of the truncated cone formed by a driven contact curve, a design of the hollow circular cylinder as the structure of a driven line gear wheel, can not only improve the strength and the stiffness of driven line gear wheel, but also lower its volume and manufacturing cost. In Fig. 4, the line teeth attached to the ektexine of a hollow truncated cone; and a hollow circular cylinder is designed for the installing of a driven axis; while a ribbed slab is designed for the connecting of a hollow truncated cone and a hollow circular cylinder.

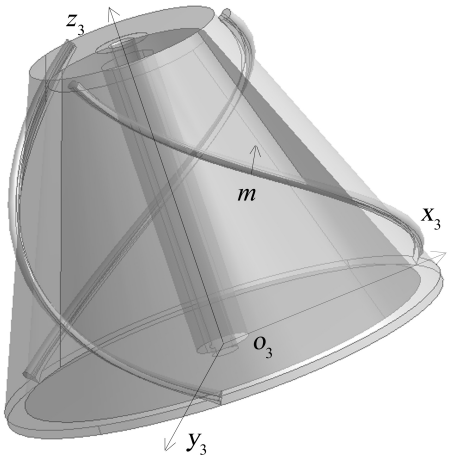

Figure 4. A hollow truncated cone is designed as a driven line gear wheel structure.

3.1 The influence of wall thickness of a hollow truncated cone on the stiffness of a line gear

3.1.1 The force analysis on the hollow truncated cone of a driven line gear

Without considering the structure and size of a ribbed slab, wall thickness δ of a hollow truncated cone is discussed in this section. In Fig. 4, the meshing force of driven line gear is different with the meshing point m as analyzed in Sect. 2. Suppose top surface 1 and bottom surface 2 of a hollow circular cylinder are fixed, according to force translation theorem of theoretical mechanics, the forces and the moments on the axis of the designated cross section, which are equivalent to the meshing forces, are obtained as Eqs. (14)–(16).

$$\begin{cases} F_{x_1} = \dfrac{F_{x3}z_{m3} + F_{z3}|x_{m3}|}{l_3} \\ F_{x_2} = \dfrac{F_{x3}(l_3 - z_{m3}) - F_{z3}|x_{m3}|}{l_3} \\ M_{x_1} = \dfrac{(F_{x3}z_{m3} + F_{z3}|x_{m3}|)(l_3 - z_3)}{l_3} \\ M_{x_2} = \dfrac{(F_{x3}(l_3 - z_{m3}) - F_{z3}|x_{m3}|)z_3}{l_3} \end{cases} \tag{14}$$

$$\begin{cases} F_{y_1} = \dfrac{F_{y3}z_{m3} + F_{z3}|y_{m3}|}{l_3} \\ F_{y_2} = \dfrac{F_{y3}(l_3 - z_{m3}) - F_{z3}|y_{m3}|}{l_3} \\ M_{y_1} = \dfrac{(F_{y3}z_{m3} + F_{z3}|y_{m3}|)(l_3 - z_3)}{l_3} \\ M_{y_2} = \dfrac{(F_{y3}(l_3 - z_{m3}) - F_{z3}|y_{m3}|)z_3}{l_3} \end{cases} \tag{15}$$

$$\begin{cases} F_{z_1} = \dfrac{F_{z3}z_{m3}}{l_3} \\ F_{z_2} = \dfrac{F_{z3}(l_3 - z_{m3})}{l_3} \\ T = \sqrt{F_{x3}^2 + F_{y3}^2}\sqrt{x_3^2 + y_3^2} \end{cases} \tag{16}$$

In Eqs. (14)–(16), the subscript of the subscript 1 refers to the top surface 1 of a hollow circular cylinder in Fig. 4, while the subscript 2 refers to the bottom surface 2 of a hollow circular cylinder in Fig. 4.

According to Eqs. (14)–(16), the strength and stiffness of the line gear wheel at different meshing point can be obtained by analysis.

3.1.2 The stiffness analysis of the hollow truncated cone of a driven line gear

The total deformation of the hollow truncated cone consists of the deformations generated by the bending moment, the torque and the axial force, respectively. The deflection equations generated by the bending moment in different directions are shown in Tables 1 and 2.

Because the results are too complex and not necessary, by substituting of different values of I_{x3} in different cross sections of a hollow truncated cone into formulae in Tables 1 and 2, I_{x3} with a fixed minimum value is set which can make the deformation maximum in this paper. By comparing this maximum deformation with an allowable material stiffness value, the wall thickness δ of the hollow truncated cone can be obtained. Meanwhile, its value is relatively safe. By this way, the deflection calculation formulae are shown in Tables 3 and 4.

The deformation generated by the torque is obtained as Eq. (17).

$$\Delta\phi = \frac{T}{GI_{\rho 3}} = \frac{\sqrt{F_{x3}^2 + F_{y3}^2}\sqrt{x_3^2 + y_3^2}}{GI_{\rho 3}} \tag{17}$$

The deformation generated by the axial force is obtained as Eq. (18).

$$\begin{aligned} \Delta z_{2_1} &= \int_{-z_{\mathrm{fe}}}^{-z_{\mathrm{m}}} \frac{F_{z_1}}{EA_{z3}}\mathrm{d}z = \frac{F_{z3}z_{m3}z_3}{El_3(\pi(R_3^2 - (R_3 - \delta)^2))} \\ \Delta z_{2_2} &= \int_{-z_{\mathrm{m}}}^{0} \frac{F_{z_2}}{EA_{z3}}\mathrm{d}z = \frac{F_{z3}(l_3 - z_{m3})z_3}{El_3(\pi(R_3^2 - (R_3 - \delta)^2))} \end{aligned} \tag{18}$$

Where, $I_{x3} = \frac{\pi\delta^2(R_3^2 + (R_3 - \delta)^2)}{4} = I_{y3}$, $I_{\rho 3} = \frac{\pi\delta^2(R_3^2 + (R_3 - \delta)^2)}{2}$.

Suppose the allowable deflection values of the hollow truncated cone of a driven line gear in x_3, y_3, z_3 directions are $[\Delta x]$, $[\Delta y]$, $[\Delta z]$ and $[\Delta\theta]$, respectively. From Tables 3,

Table 1. The deflection equation of the driven line gear in x_3 axis.

1-m part	m-2 part
$EI_{x3}\ddot{\omega_{x_1}} = M_{x_1}$	$EI_{x3}\ddot{\omega_{x_2}} = M_{x_2}$
$\dot{\omega_{x_1}} = \int_{-z_{te}}^{-z_m} \frac{M_{x_1}}{EI_{x3}} dz + C_{x_1}$	$\dot{\omega_{x_2}} = \int_{-z_m}^{-z_{ts}} \frac{M_{x_2}}{EI_{x3}} dz + C_{x_2}$
$\omega_{x_1} = \int_{-z_{te}}^{-z_m} (\int_{-z_{te}}^{-z_m} \frac{M_{x_1}}{EI_{x3}} dz + C_{x_1}) + D_{x_1}$	$\omega_{x_2} = \int_{-z_m}^{-z_{ts}} (\int_{-z_m}^{-z_{ts}} \frac{M_{x_2}}{EI_{x3}} dz + C_{x_2}) + D_{x_2}$

Table 2. The deflection equation of the driven line gear in y_3 axis.

1-m part	m-2 part
$EI_{y3}\ddot{\omega_{y_1}} = M_{y_1}$	$EI_{y3}\ddot{\omega_{y_2}} = M_{y_2}$
$\dot{\omega_{y_1}} = \int_{-z_{te}}^{-z_m} \frac{M_{y_1}}{EI_{y3}} dz + C_{y_1}$	$\dot{\omega_{y_2}} = \int_{-z_m}^{-z_{ts}} \frac{M_{y_2}}{EI_{y3}} dz + C_{y_2}$
$\omega_{y_1} = \int_{-z_{te}}^{-z_m} (\int_{-z_{te}}^{-z_m} \frac{M_{y_1}}{EI_{y3}} dz + C_{y_1}) + D_{y_1}$	$\omega_{y_2} = \int_{-z_m}^{-z_{ts}} (\int_{-z_m}^{-z_{ts}} \frac{M_{y_2}}{EI_{y3}} dz + C_{y_2}) + D_{y_2}$

and 4, Eqs. (17) and (18), Eq. (19) can be obtained.

$$
\begin{aligned}
&\delta > R_3 - \sqrt[4]{R_3^4 - 4\left(\frac{A}{\pi \Delta x E I_3}\left(\frac{l^3 z_{m3}^2}{2} - \frac{z_{m3}^3}{6}\right) - \frac{A}{3E\pi[\Delta x]} l_3 z_{m3} - \frac{A z_{m3}^2}{6EI_3\pi[\Delta x]} z_{m3} + \frac{F_{x3} z_{m3}^3}{6E\pi[\Delta x]} + \frac{F_{z3} z_{m3}^2 |x_3|}{2E\pi[\Delta x]}\right)}\\
&\delta > R_3 - \sqrt[4]{R_3^4 - 4\left(\frac{B}{EI_3\pi[\Delta x]}\left(\frac{l z_{m3}^2}{2} - \frac{z_{m3}^3}{6}\right) - \frac{B}{3E\pi[\Delta x]} l_3 z_{m3} - \frac{B z_{m3}^2}{6EI_3\pi[\Delta x]} z_{m3} + \frac{F_{y3} z_{m3}^3}{6E\pi[\Delta x]} + \frac{F_{z3} |y_3| z_{m3}^2}{2E\pi[\Delta x]}\right)}\\
&\delta > R_3 - \sqrt{R_3^2 - \left(\frac{F_{z3}(l_3 - z_{m3})}{EI_3}(z_{m3})\right)/(\pi[\Delta z])}\\
&\delta > R_3 - \sqrt[4]{R_3^4 - 2(\sqrt{F_{x3}^2 + F_{y3}^2})\sqrt{x_3^2 + y_3^2}/(G\pi[\Delta\theta])}\\
&A = F_{x3} z_{m3} + F_{z3} |x_3|\\
&B = F_{y3} z_{m3} + F_{z3} |y_3|
\end{aligned}
\tag{19}
$$

According to Eq. (19), the stiffness of the hollow truncated cone can meet the requirement.

From Fig. 1, suppose the torque of a driving line gear is equal to 2 N m, the forces and the deformations of the driven line gear wheel at different meshing point are analyzed by MATLAB, and their results are shown in Fig. 5.

Figure 5a shows the component forces' values in three axes at different meshing points; Fig. 5b shows the deformations generated by the axial force at different meshing points; Fig. 5c shows the bending deflections at different meshing points; Fig. 5d shows the deformation generated by the torque at different meshing points. From Fig. 5a, the component forces in x_3, y_3 and z_3 axes at the meshing point are not equal to one another, the changes of component forces in the x_3 and y_3 axes are periodic while the change of component force in the z_3 is monotonically increasing. From Figs. 5b–d, it is indicated that the deformation generated by the torque is maximum, and its value is 3 and 16 order of magnitudes higher than other two deformations, respectively. To simplify the calculation, the effects of the torque deformation on the driven wheel can only be considered, namely, the wall thickness of the hollow truncated cone only needs to meet Eq. (20).

$$
\delta > R_3 - \sqrt[4]{R_3^4 - 2\frac{\sqrt{F_{x3}^2 + F_{y3}^2}\sqrt{x_3^2 + y_3^2}}{G\pi[\Delta\theta]}} \tag{20}
$$

3.2 The structure design of ribbed slab structure

For more improving of the stiffness of the line gear wheel, a ribbed slab can be added between the hollow truncated cone and the hollow circular cylinder, as shown in Fig. 6. The followings discuss the structure selection and the size determination of a ribbed slab. The material of the following line gear is structural steel and its mechanic properties are $E = 2.0 \times 10^{11}$ Pa, $\mu = 0.3$, ρ=7.85 g cm^{-3}, $\sigma_s = 2.6 \times 10^8$ Pa. Their boundary conditions are the fixed upper and lower surfaces of the line gear wheels. The load distribution are applied on middle meshing point of the line teeth.

3.2.1 The structure selection of a ribbed slab

In this paper, five types of the ribbed slab structures are proposed and analyzed, as shown in Fig. 6; their volumes are equivalent, their maximum deformations and maximum equivalent stresses are analyzed by using ANSYS Workbench software, and then the optimal ribbed slab structure is determined. A ribbed slab structure in Fig. 6a consists of 5 layers of support plates: a top and a bottom circle plates and other 3 layers which every layer consists of 3 sector plates, whose sector plate's angle is equal to 45° and the midpoint of the sector plate coincides with the line tooth of driven line gear; a ribbed slab structure in Fig. 6b consists of 5 layers of support plates: a top and a bottom circle plates and other 3 layers which every layer consists of 3 sector plates and a large annulus, whose sector plate's angle is equal to 45° and the midpoint of the sector plate coincides with the line tooth of driven line gear, and whose annulus connect with hollow

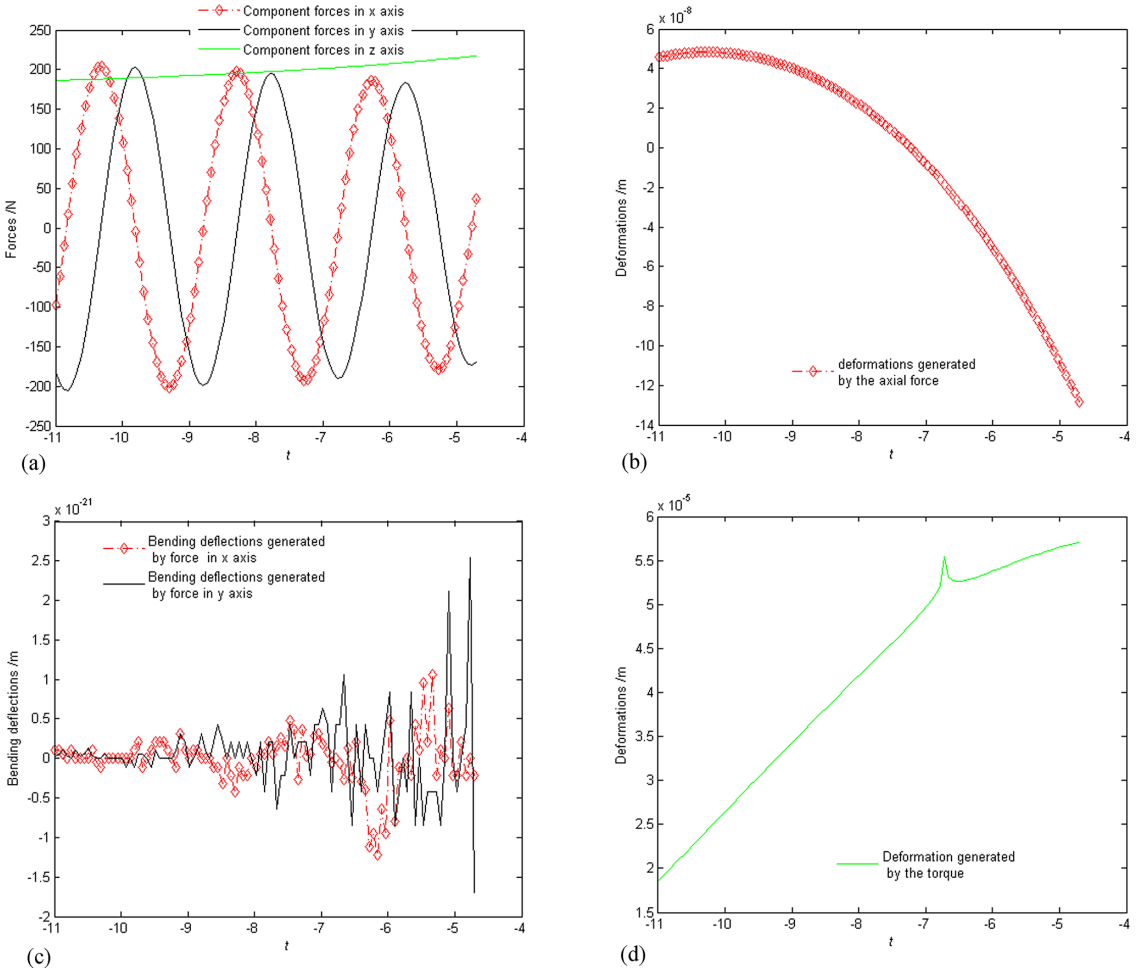

Figure 5. The forces and the deformations of the driven line gear wheel at different meshing points.

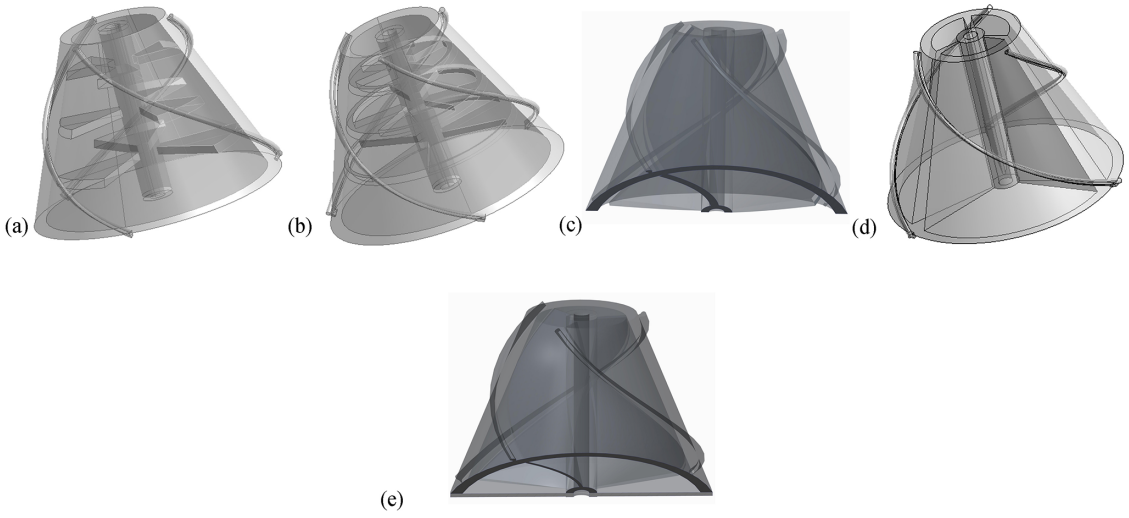

Figure 6. Five types of the ribbed slab structures of a driven line gear.

Table 3. The calculation formulae of the driven line gear in x_3 axis.

1-m part	m-2 part
$\omega_{x_1} = \frac{(F_{x3}z_{m3}+F_{z3}\lvert x_3\rvert)(3l_3z_3^2-z_3^3)}{6EI_{x3}l_3} - \frac{F_{x3}z_{m3}+F_{z3}\lvert x_3\rvert}{3EI_{x3}}l_3z_3$ $-\frac{F_{x3}z_{m3}^3+3F_{z3}z_{m3}^2\lvert x_3\rvert}{6EI_{x3}l_3}z_3 + \frac{F_{x3}z_{m3}^3}{6EI_{x3}} + \frac{F_{z3}z_{m3}^2\lvert x_3\rvert}{2EI_{x3}}$	$\omega_{x_2} = \frac{(F_{x3}(l_3-z_{m3})-F_{z3}\lvert x_3\rvert)(z_3^3)}{6EI_{x3}} - \frac{F_{z3}\lvert x_3\rvert z_{m3}^2}{2EI_{x3}l_3}z_3$ $-\frac{F_{z3}z_{m3}\lvert x_3\rvert}{EI_{x3}l_3}z_3 - \frac{F_{x3}z_{m3}^3}{6EI_{x3}l_3}z_3 - \frac{F_{x3}z_{m3}l_3}{3EI_{x3}}z_3 - \frac{F_{z3}\lvert x_3\rvert}{3EI_{x3}}l_3z_3 + \frac{F_{x3}z_{m3}^2}{2EI_{x3}}z_3$

Table 4. The calculation formulae of the driven line gear in y_3 axis.

1-m part	m-2 part
$\omega_{y_1} = \frac{(F_{y3}z_{m3}+F_{z3}\lvert y_3\rvert)(3l_3z_3^2-z_3^3)}{6EI_{y3}l_3} - \frac{F_{y3}z_{m3}+F_{z3}\lvert y_3\rvert}{3EI_{y3}}l_3z_3$ $-\frac{F_{y3}z_{m3}^3+3F_{z3}z_{m3}^2\lvert y_3\rvert}{6EI_{y3}l_3}z_3 + \frac{F_{y3}z_{m3}^3}{6EI_{y3}} + \frac{F_{z3}z_{m3}^2\lvert y_3\rvert}{2EI_{y3}}$	$\omega_{y_2} = \frac{(F_{y3}(l_3-z_{m3})-F_{z3}\lvert y_3\rvert)(z_3^3)}{6EI_{y3}l_3} - \frac{F_{z3}\lvert y_3\rvert z_{m3}^2}{2EI_{y3}l_3}z_3$ $-\frac{F_{z3}z_{m3}\lvert y_3\rvert}{EI_{y3}}z_3 - \frac{F_{y3}z_{m3}^3}{6EI_{y3}l_3}z_3 - \frac{F_{y3}z_{m3}l_3}{3EI_{y3}}z_3 - \frac{F_{z3}\lvert y_3\rvert}{3EI_{y3}}l_3z_3 + \frac{F_{y3}z_{m3}^2}{2EI_{y3}}z_3$

truncated cone; a ribbed slab structure in Fig. 6c is a impeller structure scanning by the driven center curve and shaft directly; a ribbed slab structure in Fig. 6d consists of 3 fan support plates which continuously support the hollow truncated cone; a ribbed slab structure in Fig. 6e consists of a impeller structure scanning by the driven center curve and shaft directly, and a top and a bottom circle plates. The lower of the models in Figs. 6c and d are partially fractured and their cross sections are shown gray part. The maximum deformations and the maximum equivalent stresses of the driven line gears at middle meshing point are analyzed by ANSYS Workbench, as shown in Table 5.

From Table 5, that can be concluded the ribbed slab structure in Fig. 6e is the optimal.

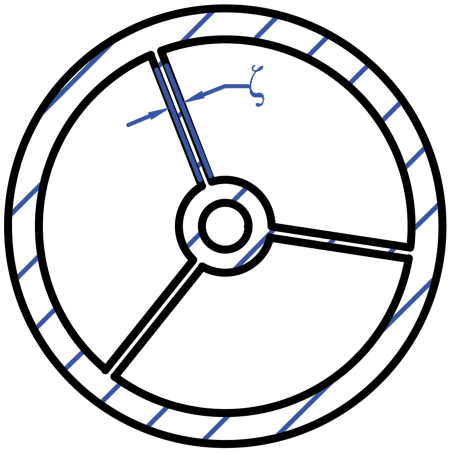

Figure 7. The cross section shape of a driven line gear in Fig. 6e.

3.2.2 Design formula of the ribbed slab on the basis of the strength criterion

The shape of the cross section of a driven line gear wheel in Fig. 6e is shown in Fig. 7. Suppose ζ is the thickness of the ribbed slab, according to the strength criterion, then ζ can be obtained.

According to Sect. 2, the bending moment, the torque and the axial force can be obtained, and the stresses generated by them are calculated by Eqs. (21)–(23).

$$\begin{cases} \tau_{F_{x_1}} = \dfrac{F_{x3}z_{m3} + F_{z3}\lvert x_{m3}\rvert}{A_{m3}l_3} \\ \tau_{F_{x_2}} = \dfrac{F_{x3}(l_3 - z_{m3}) - F_{z3}\lvert x_{m3}\rvert}{A_{m3}l_3} \\ \sigma_{M_{x_1}} = \dfrac{F_{x3}z_{m3} + F_{z3}\lvert x_{m3}\rvert}{I_{y3}l_3}(l_3 - z_3)R_{m3} \\ \sigma_{M_{x_2}} = \dfrac{F_{x3}(l_3 - z_{m3}) - F_{z3}\lvert x_{m3}\rvert}{I_{y3}l_3}(z_3)R_{m3} \end{cases} \tag{21}$$

$$\begin{cases} \tau_{f_{y_1}} = \dfrac{F_{y3}z_{m3} + F_{z3}\lvert y_{m3}\rvert}{A_{m3}l_3} \\ \tau_{f_{y_2}} = \dfrac{F_{y3}(l_3 - z_{m3}) - F_{z3}\lvert y_{m3}\rvert}{A_{m3}l_3} \\ \sigma_{M_{y_1}} = \dfrac{F_{y3}z_{m3} + F_{z3}\lvert y_{m3}\rvert}{I_{x3}l_3}(l_3 - z_3)R_{m3} \\ \sigma_{M_{y_2}} = \dfrac{F_{y3}(l_3 - z_{m3}) - F_{z3}\lvert y_{m3}\rvert}{I_{x3}l_3}(z_3)R_{m3} \end{cases} \tag{22}$$

$$\begin{cases} \tau_T = \dfrac{\sqrt{F_{x3}^2 + F_{y3}^2}\sqrt{x_3^2 + y_3^2}}{I_{\rho 3}}R_{m3} \\ \sigma_{F_{z_1}} = \dfrac{F_{z3}z_{m3}}{A_{m3}l_3} \\ \sigma_{F_{z_2}} = \dfrac{F_{y3}(l_3 - z_{m3})}{A_{m3}l_3} \end{cases} \tag{23}$$

Table 5. The statics analysis results for five types of ribbed slab structures at middle meshing point.

No.	Fore/N	Maximum deformation/m	Maximum equivalent stress/Pa	Volume/mm^3	Number of element
1	277.9429	9.4266×10^{-6}	1.7992×10^{8}	12 200	254 569
2	277.9429	1.0349×10^{-5}	1.8009×10^{8}	12 201	250 397
3	277.9429	3.2714×10^{-5}	2.6903×10^{8}	12 201	242 666
4	277.9429	9.0375×10^{-5}	3.8969×10^{8}	12 200	233 582
5	277.9429	8.79×10^{-6}	1.8359×10^{8}	12 200	270 727

where, $A_{m3} = \pi(R_{m3}^2 - (R_3 - \delta)^2) + \pi(R_{z3}^2 - r_{z3}^2) + 3\zeta(R_3 - \delta - R_{z3})$. According to Sect. 2.1, δ can be decided. Because the shape of the cross section of a driven line gear wheel is irregular, the calculations of the inertia moment and the polar moment of inertia are relatively complex. Using the calculation method that the irregular cross section is divided into several regular sections, the inertia moment and the polar moment of inertia in Eqs. (21)–(23) can be obtained by using Eqs. (24)–(26).

$$I_{y3} = \int x_3^2 \mathrm{d}A = \frac{\pi\delta^2(R_3^2 + (R_3 - \delta)^2)}{4} + \frac{\pi(R_{z3}^4 - r_{z3}^4)}{4} + \frac{\zeta((R_3 - \delta) - R_{z3})^3}{2} \tag{24}$$

$$I_{x3} = \int y_3^2 \mathrm{d}A = \frac{\pi\delta^2(R_3^2 + (R_3 - \delta)^2)}{4} + \frac{\pi(R_{z3}^4 - r_{z3}^4)}{4} + \frac{\zeta((R_3 - \delta) - R_{z3})^3}{2} \tag{25}$$

$$I_{\rho 3} = \frac{\pi\delta^2(R_3^2 + (R_3 - \delta)^2)}{2} + \frac{\pi(R_{z3}^4 - r_{z3}^4)}{2} + \zeta((R_3 - \delta) - R_{z3})^3 \tag{26}$$

The shear stresses generated by two component forces in x_3 and y_3 axes respectively are relatively so small that they can be ignored. According to knowledge of material mechanics, comprehensively considering the bending moment, the axial force and the torque, the dangerous section of a driven line gear wheel may occur in the force bearing point, because this point bears the biggest bending moment. Meanwhile it bears the axial force and torque. Therefore, in the maximum stress point, the stress state is 2-D stress produced by the bending moment, the torque and the axial force, as shown in Fig. 8.

The principal stresses can be obtained by using Eq. (27).

$$\left.\begin{matrix}\sigma_1 \\ \sigma_3\end{matrix}\right\} = \frac{\sqrt{\sigma_y^2 + \sigma_x^2} + \sigma_{F_z}}{2} \pm \sqrt{\left(\frac{\sqrt{\sigma_y^2 + \sigma_x^2} + \sigma_{F_z}}{2}\right)^2 + \tau_T^2} \tag{27}$$

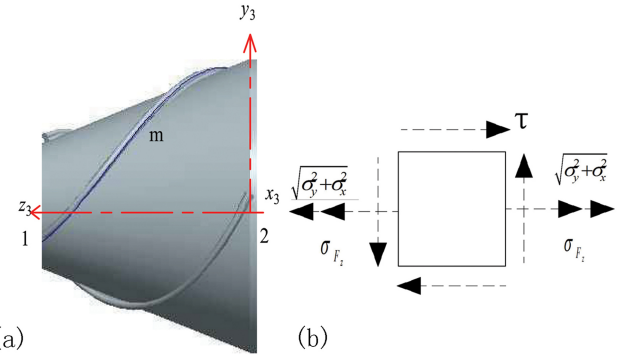

Figure 8. The diagram of shear stress and normal stress of maximum stress unit point.

According to the maximum shear stress theory (James and Barry, 2011), Eq. (28) can be obtained.

$$\sigma_1 - \sigma_3 \le \frac{\sigma_s}{n_s} \tag{28}$$

According to Eqs. (21)–(24), Eq. (29) can be obtained.

$$\left.\begin{matrix}\sigma_1 \\ \sigma_3\end{matrix}\right\} = \frac{\sqrt{\left(\frac{C}{I_{x3}I_{y3}}(l_3 - z_{m3})R_{m3}\right)^2 + \left(\frac{D}{I_{x3}I_{y3}}(l_3 - z_{m3})R_{m3}\right)^2} + \frac{F_{z3}z_{m3}}{A_{m3}I_{y3}}}{2} \pm \sqrt{\left(\frac{\sqrt{\left(\frac{C}{I_{x3}I_{y3}}(l_3 - z_{m3})R_{m3}\right)^2 + \left(\frac{D}{I_{x3}I_{y3}}(l_3 - z_{m3})R_{m3}\right)^2} + \frac{F_{z3}z_{m3}}{A_{m3}I_{y3}}}{2}\right)^2 + \left(\frac{\sqrt{F_{x3}^2 + F_{y3}^2}\sqrt{x_3^2 + y_3^2}}{I_{\rho 3}}R_{m3}\right)^2} \tag{29}$$

$C = F_{y3}z_{m3} + F_{z3}|y_{m3}|$
$D = F_{x3}z_{m3} + F_{z3}|x_{m3}|$

Substituting Eq. (29) into Eq. (28), Eq. (30) can be obtained.

$$2\sqrt{\left(\frac{\sqrt{\left(\frac{C}{I_{x3}I_{y3}}(l_3 - z_{m3})R_{m3}\right)^2 + \left(\frac{D}{I_{x3}I_{y3}}(l_3 - z_{m3})R_{m3}\right)^2} + \frac{F_{z3}z_{m3}}{A_{m3}I_{y3}}}{2}\right)^2 + \left(\frac{\sqrt{F_{x3}^2 + F_{y3}^2}\sqrt{x_3^2 + y_3^2}}{I_{\rho 3}}R_{m3}\right)^2} \le \frac{\sigma_s}{n_s} \tag{30}$$

$C = F_{y3}z_{m3} + F_{z3}|y_{m3}|$
$D = F_{x3}z_{m3} + F_{z3}|x_{m3}|$

Using Eqs. (27)–(30), the minimum thickness of a ribbed slab can be obtained.

3.3 The design formulae of the thicknesses of a top circle plate and a bottom circle plate

By comparing Fig. 6c with Fig. 6e, a conclusion can be drawn that the structure with a top circle plate and a bottom circle plate is better than the one without circle plates,

Table 6. The statics analysis results at middle meshing point, without equivalent thicknesses of a top circle plate and a bottom circle plate

No.	Fore/N	Maximum deformation/m	Maximum equivalent stress/Pa	Volume /mm^3	Thickness of upper plate/mm	Thickness of lower plate/mm	Number of element
1	277.9429	8.2071×10^{-6}	1.8762×10^{8}	12 198	0.8	0.8	274 546
2	277.9429	6.1809×10^{-6}	1.3742×10^{8}	12 199	1.8	0.695	271 378
3	277.9429	5.7629×10^{-5}	1.3722×10^{8}	12 198	2.635	0.6	264 901
4	277.9429	5.7386×10^{-6}	1.4917×10^{8}	12 199	0.5	3.43	261 578
5	277.9429	8.697×10^{-6}	1.9875×10^{8}	12 200	0.695	0.812	271 905
6	277.9429	9.3746×10^{-6}	2.0093×10^{8}	12 201	0.6	0.6	270 727
7	277.9429	7.7317×10^{-6}	1.6682×10^{8}	12 200	0.717	0.717	268 402

for a design of equivalent volume of the driven line gear wheel, and the equivalent wall thickness of the hollow truncated cone. Meanwhile, a larger additional wind loads may be produced by the high speed rotating of the driven line gear wheel, with a structure in Fig. 6c, that may cause the harmful effects such as vibration and noise. In this section, the design formulae for the thicknesses of a top circle plate and a bottom circle plate are deduced.

The statics analysis results at middle meshing point, without equivalent thicknesses of a top circle plate and a bottom circle plate, are shown in Table 6.

According to Table 6, when thickness of a top circle plate is large than the thickness of a bottom circle plate, the maximum deformation and the maximum equivalent stress of a driven line gear are the smallest. Therefore, in this paper, the relationship between the thickness of the top circle plate η and thickness of a bottom circle plate ξ is set as $\eta = 4\xi$, while the relationship between ξ and height of a driven line gear wheel is set as $l_3 = 60\xi$.

3.4 Design of a hollow circular cylinder for the installation of the driven axis

The inner diameter of a hollow circular cylinder depends on the output torque. When the inner diameter of a hollow circular cylinder $r_{z3} < (R_{3_1} - s) - 5$, the structure of the driven line gear wheel can be designed as a structure shown in Fig. 6e, and an outer diameter of the hollow circular cylinder is $R_{z3} = r_{z3} + 3$; but for that case $r_{z3} \le (R_{3_1} - s) - 5$, the structure of a driven line gear wheel can be designed in the entity type.

3.5 The calculation formulae for the stiffness and strength of a driving line gear wheel

A driving line gear wheel is designed as an entity type, namely, it is a cylinder. The driving line tooth is ignored, and only the wheel is considered here, then its strength calculation formulae can be also from Tables 3, 4, Eqs. (17) and (18). Because its cross section shape is not equivalent to a driven line gear wheel, its inertia moment and the polar moment of inertia can be calculated by $I_{x1} = I_{y1} = \pi R_1^4/4$ and $I_{\rho 1} = \pi R_1^4/2$, respectively. Its maximum deformation can be calculated by Eqs. (31)–(35).

$$\begin{aligned}\Delta y = {} & 4\frac{(F_{x1}z_{m1} + F_{z1}|x_{m1})(3l_1 z_{m1}^2 - z_{m1}^3)}{6El_1\pi R_1^4} \\ & - 4\frac{F_{x1}z_{m1} + F_{z1}|x_{m1}|}{3E\pi R_1^4} l_1 z_{m1} \\ & - 4\frac{F_{x1}z_{m1}^3 + 3F_{z1}z_{m1}^2|x_{m1}|}{6El_1\pi R_1^4} z_{m1} \\ & + 4\frac{F_{x1}z_{m1}^3}{6E\pi R_1^4} + 4\frac{F_{z1}z_{m1}^2|x_{m1}|}{2E\pi R_1^4}\end{aligned} \tag{31}$$

$$\begin{aligned}\Delta x = {} & 4\frac{(F_{y1}z_{m1} + F_{z1}|y_{m1})(3l_1 z_{m1}^2 - z_{m1}^3)}{6El_1\pi R_1^4} \\ & - 4\frac{F_{y1}z_{m1} + F_{z1}|y_{m1}|}{3E\pi R_1^4} l_1 z_{m1} \\ & - 4\frac{F_{y1}z_{m1}^3 + 3F_{z1}z_{m1}^2|y_{m1}|}{6El_1\pi R_1^4} z_{m1} \\ & + 4\frac{F_{y1}z_{m1}^3}{6E\pi R_1^4} + 4\frac{F_{z1}z_{m1}^2|y_{m1}|}{2E\pi R_1^4}\end{aligned} \tag{32}$$

$$\Delta z = \frac{F_{z1}(l_1 - z_{m1})z_{m1}}{\pi E l_1 R_1^2} \tag{33}$$

$$\Delta\theta = 360\frac{\sqrt{F_{x1}^2 + F_{y1}^2}\sqrt{x_1^2 + y_1^2}}{\pi^2 R_1^4} \tag{34}$$

$$\begin{aligned}\left.\begin{matrix}\sigma_1 \\ \sigma_3\end{matrix}\right\} = {} & \frac{\sqrt{\left(\frac{A_1}{I_{x1}l_1}(l_1 - z_{m1})R_{m1}\right)^2 + \left(\frac{B_1}{I_{y1}l_1}(l_1 - z_{m1})R_{m1}\right)^2} + \frac{F_{z1}z_{m1}}{A_{m1}l_1}}{2} \pm \\ & \sqrt{\left(\frac{\sqrt{\left(\frac{A_1}{I_{x1}l_1}(l_1 - z_{m1})R_{m1}\right)^2 + \left(\frac{B_1}{I_{y1}l_1}(l_1 - z_{m1})R_{m1}\right)^2} + \frac{F_{z1}z_{m1}}{A_{m1}l_1}}{2}\right)^2 + \frac{(F_{x1}^2 + F_{y1}^2)(x_1^2 + y_1^2)}{I_{\rho 1}}R_{m1}^2} \\ A_1 = {} & F_{y1}z_{m1} + F_{z1}|y_{m1}| \\ B_1 = {} & F_{x1}z_{m1} + F_{z1}|x_{m1}|\end{aligned} \tag{35}$$

Table 7. Basic dimension parameters of a skewed line gear pair.

Symbol	Definition	Computational formula	Computational formula
θ	Angle between two angular velocity	$0° < \theta < 90°$	$90° < \theta < 180°$
$\|c\|$ (mm)	The distance of two skewed axes	Given	Given
i	Transmission ratio	Given	Given
m (mm)	Meshing radius of driving contact curve	Given	Given
n (mm)	Pitch coefficient of driving contact curve	$n \geq \max(0, \frac{cm\sin\theta - m^2\sin\theta}{mi + m\cos\theta - c\cos\theta})$	$n \geq \max(0, \frac{-cm\sin\theta + m^2\sin\theta}{mi - m\cos\theta + c\cos\theta})$

Table 8. Calculated dimensional parameters of a skewed line gear pair.

Symbol	Definition	Computational formula	Computational formula
θ	Angle between two angular velocity	$0° < \theta < 90°$	$90° < \theta < 180°$
$\|a\|$ (mm)	Distance from point o_p to z axis	$a = nt_s\cos\theta\sin\theta - (\cos(\phi_{1s} - t_s)m)\sin^2\theta$	$a = nt_s\cos\theta\sin\theta - (\cos(\phi_{1s} - t_s)m)\sin^2\theta$
$\|b\|$ (mm)	Distance from point o_p to x axis	$b = \frac{a\cos\theta}{\sin\theta} + n\pi$	$b = \frac{a\cos\theta}{\sin\theta} + n\pi$
t_m	Middle meshing point	$f(t_m) = 0$	$f(t_m) = 0$
t_s	Initial meshing point	$t_s \geq 0; t_m = (t_s + t_e)/2; t_e - t_s = \pi/2$	$t_m = (t_s + t_e)/2; t_e - t_s = \pi/2$
t_e	Ending meshing point	$t_m = (t_s + t_e)/2; t_e - t_s = \pi/2$	$t_s \leq 0; t_m = (t_s + t_e)/2; t_e - t_s = \pi/2$

According to the strength standard $\sigma_1 - \sigma_3 \leq \sigma_s/n_s$, the values of n and m can be calculated and adjusted.

According to Eqs. (31)–(35), the maximum deformation and the maximum stress of a driving line gear can be obtained.

4 Parameters standardization formulae for a skewed line gear pair when the number of a driving line tooth is 1

The basic dimension parameters of a skew line gear pair are shown in Table 7.

Furthermore, the calculated dimensional parameters of a skew line gear pair are shown in Table 8. When $0° < \theta < 90$, $f(t) = mi + m\cos\theta + c\sin(\phi_1 - t)\cos\theta + nt\sin\theta\cos(\phi_1 - t) - m\sin\theta(m\sin(\phi - t) + c)/n$; when $90° < \theta < 180°$, $f(t) = mi - m\cos\theta - c\sin(\phi_1 - t)\cos\theta - nt\sin\theta\cos(\phi_1 - t) + m\sin\theta(m\sin(\phi - t) + c)/n$.

Then, the dimension calculation formulae of a driven line gear wheel can be obtained, as shown in Table 9.

While the dimension calculation formulae of a driving line gear wheel can be obtained, as shown in Table 10.

Where r is the radius of the driving line tooth, and its value is in the range of 1–5 mm in this paper. Its value can be calculated on basis of the bending strength and meshing stiffness of the line tooth, which is not presented in this paper.

5 A design example

In this section, a skewed line gear pair is designed according to Tables 7–10. The line gear material is structural steel, according to Cheng (2004a, b), its characteristics is $E = 2.0 \times 10^{11}$ Pa; $\mu = 0.3$; $\sigma_s = 2.6 \times 10^8$ Pa; $[\Delta x] = 0.0002$–0.0005 m; $[\Delta y] = 0.0002$–0.0005 m; $[\Delta z] = 0.0002$–0.0005 m; $[\Delta\theta] = 0.05° \text{ m}^{-1}$. The basic dimension parameters of the designed line gear pair are as follows: $c = 30$ mm; $\theta = 120°$; $i = 1/4$; $T_1 = 98$ N m; $r = 0.8$ mm; selected primary parameters are: $n = 12$ mm; $m = 10$ mm. From Table 8, $a = 55.354$ mm; $b = 5.7040$ mm; $t_m = -1.937\pi$; $t_s = -2.937\pi$; $t_e = -0.937\pi$. When $t_m = -1.937\pi$, the deformation of the driving line gear wheel is the largest, and the component forces at that time are $F_{x1} = -1.0286 \times 10^3$ N; $F_{y1} = 5.1292 \times 10^3$ N; $F_{z1} = -4.3594 \times 10^3$ N; $l_1 = 75.3982$ mm; $R_1 = 9.28$ mm. Therefore, according to Eq. (32), results can be obtained as: $\sigma_1 = 3.645397 \times 10^8$ Pa; $\sigma_3 = -3.0425 \times 10^6$ Pa; $\sigma_1 - \sigma_3 > \sigma_s$, which means, this design is not reasonable. The value of m must be adjusted. Setting $m = 13$ mm; $n = 17$ mm; $r = 1.6$ mm; then $a = 70.4052$ mm; $b = 12.7586$ mm; $t_m = -1.626\pi$; $t_s = -2.626\pi$; $t_e = -0.626\pi$. When $t_m = -1.626\pi$, the deformation of the driving line gear wheel is the largest, and the component forces at that time are $F_{x1} = -0.84002 \times 10^3$ N; $F_{y1} = 4.1887 \times 10^3$ N; $F_{z1} = -3.2669 \times 10^3$ N; $R_1 = 12.28$ mm; $l_1 = 106.8$ mm. Therefore, according to Eq. (32), results can be obtained as followings: $\sigma_1 = 1.897449 \times 10^8$ Pa; $\sigma_3 = -1.3649 \times 10^6$ Pa; $\sigma_t = \sigma_1 - \sigma_3 < \sigma_s/n_s$, where $n_s = 1.36$. From Tables 9 and 10, results can be obtained as followings: $R_{max3} = 117.9$ mm; $R_{min3} = 35.1$ mm; $l_3 = 53.2$ mm; $\delta = 1.5$ mm; $\zeta = 1.9$ mm; $r_{z3} = 13$ mm; $R_{z3} = 16$ mm; $\eta = 3.53$ mm; $\xi = 0.89$ mm. The structure of a skewed line gear pair can be completely drawn by using these dimension values, as shown in Fig. 9.

Using finite element analysis on ANSYS Workbench to analyze the models in Fig. 9 with two head faces of the line gear wheel fixed as boundary condition, the statics analysis

Table 9. The dimension calculation formulas of a driven line gear wheel.

Symbol	Definition	Computational formula	Computational formula
θ	Angle between two angular velocity	$0° < \theta < 90°$	$90° < \theta < 180°$
$R_{\min 3}$ (mm)	Small side radius of driven line gear wheel	$\sqrt{(x_3(t_e))^2 + (y_3(t_e))^2}$	$\sqrt{(x_3(t_s))^2 + (y_3(t_s))^2}$
$R_{\max 3}$ (mm)	Large side radius of driven line gear wheel	$\sqrt{(x_3(t_s))^2 + (y_3(t_s))^2}$	$\sqrt{(x_3(t_e))^2 + (y_3(t_e))^2}$
l_3 (mm)	Height of the driven line gear wheel	$z_{3s} - z_{3e}$	$z_{3e} - z_{3s}$
α_1	Angle of the hollow truncated cone of driven line gear	$\arctan \frac{\lvert R_{\max 3} - R_{\min 3} \rvert}{l_3}$	$\arctan \frac{\lvert R_{\max 3} - R_{\min 3} \rvert}{l_3}$
δ	Thickness of hollow truncated cone	Eq. (20)	Eq. (20)
ζ	Thickness of ribbed slab	Eq. (27)	Eq. (27)
r_{z3} (mm)	The hollow circular cylinder inner diameter	depend on the output shaft torque	depend on the output shaft torque
R_{z3} (mm)	The hollow circular cylinder outer diameter	$R_{z3} = r_{z3} + 3$	$R_{z3} = r_{z3} + 3$
η	Thickness of upper plate	$\eta = 4\xi$	$\eta = 4\xi$
ξ	Thickness of lower plate	$\xi = l_3/60$	$\xi = l_3/60$

Table 10. The dimension calculation formulae of a driving line gear wheel.

Symbol	Definition	Computational formula
R_1 (mm)	Radius of driving line gear wheel	$m - 0.9r$
l_1 (mm)	Height of driving line gear wheel	$z_{1e} - z_{1s}$

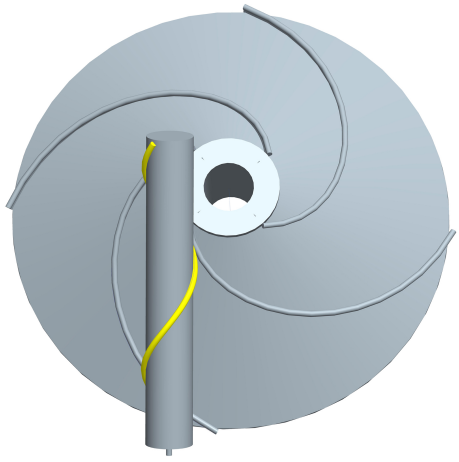

Figure 9. Design example.

results of the designed skewed line gear pair are obtained, as shown in Fig. 10. Figure 10a and b show the deformation and the equivalent stress of the driving line gear, respectively, while Fig. 10c and d show the deformation and the equivalent stress of the driven line gear, respectively. In Fig. 10a and b, the maximum deflection of the driving line gear is 9.5496×10^{-6} m, while the maximum equivalent stress of the driving line gear is 1.0578×10^8 Pa. According to the characteristics of the material, the allowable stress is $\sigma_s = 2.6 \times 10^8$ Pa, so the designed driving line gear conforms to the requirements of the strength. The simulation value 1.6507×10^8 Pa is less than the calculated value $\sigma_t = 1.911098 \times 10^8$ Pa, because the line teeth make the value of inertia moment to be larger than the calculated value. In Fig. 10c and d, the maximum deflection of the driven line gear is 6.8464×10^{-5} m, while the maximum equivalent stress of the driven line gear is 1.1004×10^8 Pa, which are both less than the allowable values of material properties. Therefore, using this method to design a skewed line gear wheel structure can meet the requirements of the strength and the stiffness in practical application. By the way, the maximum equivalent stress and the maximum deformation in Fig. 10 are mainly concentrated in the line tooth, so the maximum equivalent stress and the maximum deformation of the line gear wheels are smaller than the displayed one on ANSYS Workbench. As for the bending strength, the meshing stiffness and the dimension calculation, they are not discussed in this paper due to the paper length and will be discussed in subsequent papers.

6 Conclusions

By means of analyzing the meshing forces of the skewed line gears, their formulae at the different meshing points are obtained, and the deformations and the equivalent stresses of the existing structures of the driving and the driven line gears, when the number of a driving line tooth is equal to 1, are calculated by using ANSYS Workbench. Based on the analyzed results, a conclusion can be drawn that the transmission moment of the existing structure of line gear is relatively small and suitable neither for the driving line gear which line tooth number equals to 1 nor for the traditional powered transmission field. By the researches in this paper, oriented to additive manufacturing technology, when the number of a driving line tooth equals to 1, the structure of a driven line gear wheel can be designed as a hollow truncated cone with im-

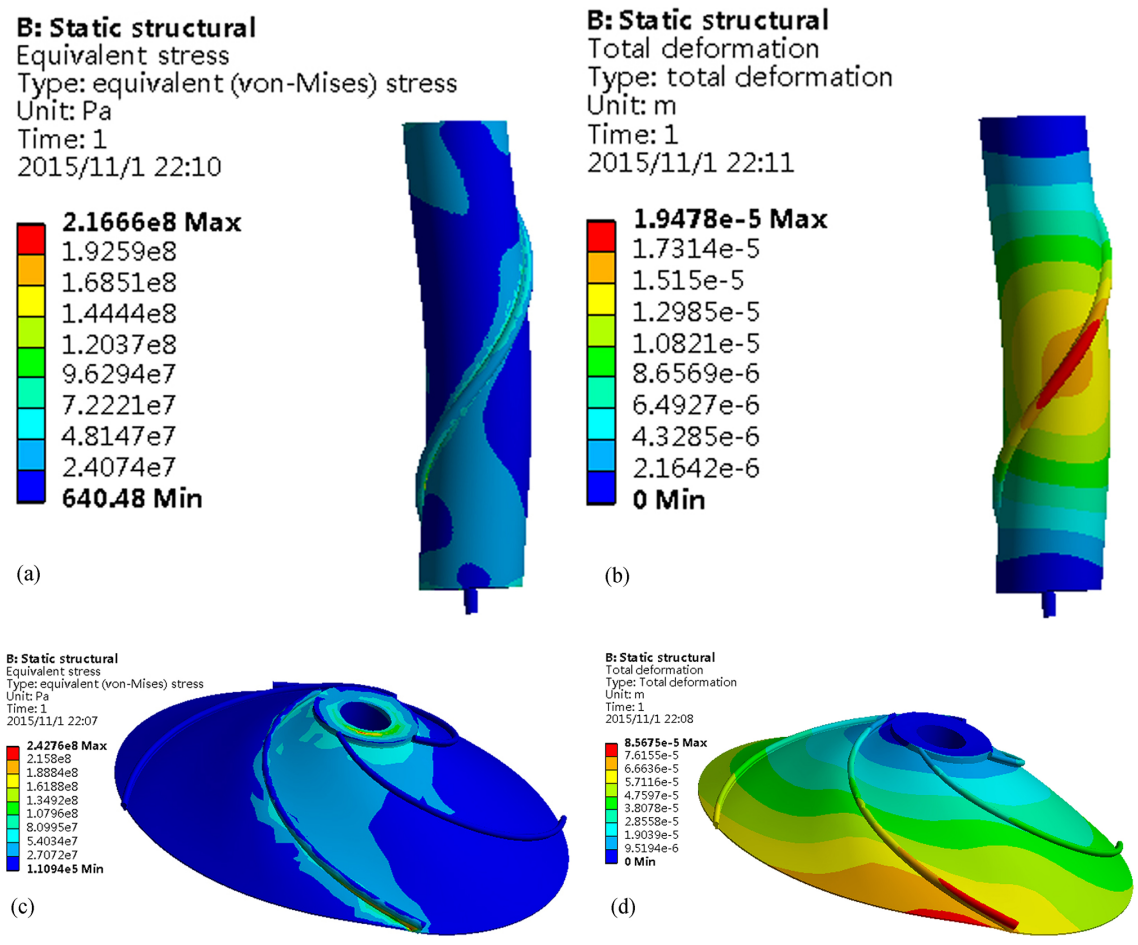

Figure 10. Statics analysis of the designed skewed line gear pair.

peller shape as ribbed slab. And the thickness formulae of a hollow truncated cone and a ribbed slab are derived on basis of their stiffness and strength calculation. Other parameter calculation experience formulae for the line gear wheels are derived by using ANSYS Workbench. Then the structural design of the skew line gear wheels is accomplished, which can be applied in large transmission torque application occasion. A design example of a skew line gear pair shows design processes of a skew line gear pair which number of driving line tooth equals to 1 and verify the accuracy of the parameter calculation formulae proposed by this paper. Although the parameters calculation formulae of the skewed line gear wheels are obtained in this paper, the specific parameter design, the bending strength and the meshing stiffness of the line tooth has not been discussed yet and will be researched in depth in the next paper.

Data availability. No data sets were used in this article.

Appendix A: Notation and units

$\|a\|$	Distance from point o_q to axis z (mm)
$\|b\|$	Distance from point o_q to axis x (mm)
$\|c\|$	Distance from point o_q to axis y (mm)
E	Modulus of Elasticity (Pa)
$F_n^{(0)}$	The meshing force on a driving line tooth at the meshing point (N)
$F_3^{(q)}$	The meshing force on a driven line tooth at the meshing point (N)
i_{21}	Transmission ratio
l_1	Height of driving line gear wheel (mm)
l_3	Height of driven line gear wheel (mm)
m	Helix radius of driving curve (mm)
$\mathbf{M}_{31}$	Transformation matrix from $o_1 - x_1y_1z_1$ to $o_3 - x_3y_3z_3$
n	Pitch parameter of driving curve (mm)
r	Radius of driving and driven line teeth (mm)
r_{z3}	The hollow circular cylinder inner diameter (mm)
R_1	Radius of driving line gear wheel (mm)
$R_{\min 3}$	Small side radius of driven line gear wheel (mm)
$R_{\max 3}$	Large side radius of driven line (mm)
R_{z3}	The hollow circular cylinder outer diameter (mm)
t_m	Middle meshing point
t_s	Initial meshing point
t_e	Ending meshing point
T_1	The torque of the driving line gear (Nm)
θ	Included angle between angular velocity vectors (°)
α_1	Angle of the hollow truncated cone of driven line gear (°)
δ	Thickness of hollow truncated cone (mm)
ζ	Thickness of ribbed slab (mm)
η	Thickness of upper plate (mm)
ξ	Thickness of lower plate (mm)
μ	Thickness of upper plate (mm)
σ_s	Yield strength (Pa)

Competing interests. The authors declare that they have no conflict of interest.

Acknowledgements. The authors thank the support from the National Natural Science Foundation of China (Item No. 51175180, No. 51575191), China Postdoctoral Science Foundation (No. 2017M612652) and Central university basic scientific research service fee (No. 2017B0071). It is our honor to thank the reviewers and editors for their valuable criticisms and comments.

Edited by: Chin-Hsing Kuo
Reviewed by: two anonymous referees

References

Chang, S. H., Chung, T. D., and Lu, S. S.: Tooth contact analysis of face-gear drives, Int. J. Mech. Sci., 42, 487–502, 2000.

Chen, Y. Z.: Line Gear, Science Press of China, Beijing, China, 2014.

Chen, Y. Z. and Chen, Z.: Contact ratio of spatial helix gearing mechanism, Proceedings of the ASME 2012 International Mechanical Engineering Congress and Exposition (IMECE2012), Houston, Texas, USA, 1529–1536, 9–15 November 2012.

Chen, Y. Z., Xiang, X. Y., and Luo, L.: A corrected equation of space curve meshing, Mech. Mach. Theory, 44, 1348–1359, 2009.

Chen, Z., Chen, Y. Z., and Ding, J.: A generalized space curve meshing equation for arbitrary intersecting gear, P. I. Mech. Eng. C-J. Mec., 227, 1599–1607, 2013a.

Chen, Y. Z., Lv, Y. L., Ding, J., and Chen, Z.: Fundamental design equations for space curve meshing skew gear mechanism, Mech. Mach. Theory, 70, 175–188, https://doi.org/10.1016/j.mechmachtheory.2013.07.004, 2013b.

Cheng, D. X.: Machinerys Handbook (Commonly used engineering materials), Chemical Industry Press, Beijin, China, 2004a.

Cheng, D. X.: Machinerys Handbook (Axle and its connection), Chemical Industry Press, Beijin, China, 2004b.

Frederik, V., Wesley, V., Andre, V., and Hans, V.: An initial study of aerosol jet® printed interconnections on extrusion-based 3D-printed substrates, Strojniski Vestnik – J. Mech. Eng., 59, 689–696, 2013.

Huang, C., Wang, J. X., Xiao, K., Li, M., and Li, J. Y.: Dynamic characteristics analysis and experimental research on a new type planetary gear apparatus with small tooth number difference, J. Mech. Sci. Technol., 27, 1233–1244, 2013.

James, M. G. and Barry, J. G.: Strength of materials, China Machine Press, Beijing, China, 2011.

Lv, Y. L., Chen, Y. Z., and Cui, X. Y.: A contact ratio and interference-proof conditions for a skew line gear mechanism, T. Can. Soc. Mech. Eng., 39, 647–656, 2015.

Patil, S. S., Karuppanan, S., Atanasovska, I., and Wahab, A. A.: Contact stress analysis of helical gear pairs, including frictional coefficients, Int. J. Mech. Sci., 85, 205–211, 2014.

Pedrero, J. I., Vallejo, I. I., and Pleguezuelos, M.: Calculation of tooth bending strength and surface durability of high transverse contact ratio spur and helical gear drives, ASME J. Mech. Design, 129, 69–74, 2007.

Wei, J., Sun, W., and Wang, L.: Effects of flank deviation on load distributions for helical gear, J. Mech. Sci. Technol., 25, 1781–1789, 2011.

Yang, Y. Q., He, X. R., Wu, W. H., Ding, H. W., Wang, D., Sun, T., and Huang, W. H.: Direct manufacturing of customized orthopedics surgery orienting model by selective laser melting, Chinese J. Lasers, 36, 2460–2464, https://doi.org/10.3788/CJL20093609.2460, 2009.